Resonance-excitation process for Ni-like tantalum

T. M. Shen,[1,2] C. Y. Chen,[1,2,*] Y. S. Wang,[1,2] and Y. M. Zou[1,2]
[1]*Shanghai EBIT Lab, Modern Physics Institute, Fudan University, Shanghai 200433, China*
[2]*The Key Lab of Applied Ion Beam Physics, The Ministry of Education, Fudan University, Shanghai 200433, China*

M. F. Gu[†]
Department of Physics, Stanford University, Stanford, California 94305, USA
(Received 14 February 2007; published 6 August 2007)

A detailed large-scale calculation on the resonant excitation rate coefficients from the ground state to the 106 fine-structure levels belonging to $3l^{17}4l'$ ($l=0,1,2$; $l'=0,1,2,3$) configurations of Ni-like tantalum have been performed using the relativistic distorted-wave approximation. The contributions through all possible Cu-like doubly excited states $3l^{17}4l'n''l''$ and $3l^{17}5l'n''l''$ ($n''\leqslant 15$, $l''\leqslant 8$) are calculated. The validity of n''^{-3} scaling law is investigated. The radiative damping effects on resonant excitation rates are studied. The significant effects arising from decays to autoionizing levels are also investigated. The contributions from resonant excitation are found to be as important as direct excitation processes for most transitions. In some cases, the resonant excitation can enhance the excitation rate coefficients by an order of magnitude. Large discrepancies between the present resonant excitation rate coefficients with previously published values are found, and the present results should be more reliable and accurate.

DOI: 10.1103/PhysRevA.76.022703 PACS number(s): 34.80.Dp, 34.80.Kw, 34.80.Lx

I. INTRODUCTION

Ni-like tantalum ion has been demonstrated to achieve amplification in the soft x-ray regime by an electron collisional excitation scheme [1]. In order to correctly model the high-temperature plasmas relevant to x-ray lasers design, as well as astrophysics and fusion research, one needs vast amounts of atomic data. Especially, excitation rate coefficients with high quality are needed since electron-impact excitation is the mechanism that produces the inversion. In high-Z materials ionized into open M- or N-shell configurations, two electron processes such as resonant capture, play an important role by adding significant channels to ionization, excitation, and recombination through multiply excited states. It has been found that the theoretical charge-state distribution agrees with that from the experiment only when two electron processes are included [2]. Resonant capture can be stabilized by two mutually competing processes: autoionizing decay leading to resonance excitation (RE) and radiative decay leading to dielectronic recombination (DR). Auger decay back to the initial state of the resonant capture results in elastic scattering and can be treated as autoionizing loss for both RE and DR.

Recently, measurements for cross sections of highly ionized Ni-like ions became possible by using the high-resolution broadband coverage of the Goddard Space Flight Center microcalorimeter in combination with an electron beam ion trap [3]. The preliminary results indicate that in some cases discrepancies with the theory including only contributions from direct excitation may be as large as 30% for Ni-like gold [3]. It is of interest to compare theoretical results with future measured ones for other Ni-like ions.

Relativistic distorted-wave calculations of collision strengths for Ni-like ions have been performed by Hagelstein [4], Zhang *et al.* [5,6], and Zhong *et al.* [7,8] without consideration of resonant contributions. The excitation rate coefficients including RE contributions are reported recently for a few Ni-like ions. Aggarwal *et al.* [9–11] carried out studies on excitation rate coefficients of transitions among the lowest 59 levels of Gd^{36+} by using the Dirac atomic R-matrix code. In 2004, Badnell *et al.* [12] carried out a 129-level close-coupling Dirac-Coulomb R-matrix calculation for the electron-impact excitation of Xe^{26+}. In 2006, Ballance *et al.* [13] presented the relativistic radiatively damped R-matrix calculation of the electron-impact excitation among the selected 115 levels of W^{46+}. By using distorted-wave and multiconfiguration Dirac-Fock (MCDF) methods, Chen and Osterheld [14] calculated DE and RE rate coefficients from the ground state to the 54 fine-structure levels belonging to $3d^94l$ configurations of Ta^{45+}. Contributions through the Cu-like doubly excited states of $3s^23p^53d^{10}4l'nl''$ and $3s^23p^63d^95l'nl''$ ($n=5-9$, $l''\leqslant 4$) associated with $3p\rightarrow 4l'$ and $3d\rightarrow 5l'$ core excitations were calculated explicitly while those from high-n Rydberg states were taken into account using the n^{-3} scaling law. Fournier *et al.* [15] calculated rate coefficients of resonant excitation into the levels of the $3d^94s$ and $3d^94p$ configurations of Mo^{14+} using a fully relativistic, multiconfiguration atomic structure code RELAC [16]. In Ref. [15], contributions through complexes series $3p^63d^94lnl''$ ($l\leqslant 3$; $5\leqslant n\leqslant 12$; $l''\leqslant 5$) and $3p^53d^{10}4lnl''$ ($l\leqslant 3$; $4\leqslant n\leqslant 10$; $l''\leqslant 5$) of Mo^{13+} were included explicitly while considering high-n contributions also by the n^{-3} scaling law. Large resonant enhancements up to an order of magnitude were observed from the above calculations. It should be pointed out that the close-coupling expansions of the Ni-like targets differ from each other among the above R-matrix calculations [9–13]. In the two distorted-wave calculations

*Author to whom correspondence should be addressed; chychen@fudan.edu.cn
†Present address: Lawrence Livermore National Laboratory, Livermore, CA 94550, USA.

[14,15], resonant configurations taken into account are associated with different core excitations and different ranges of l'' values (the orbital angular momentum of the captured electron), and the extrapolations begin from different n values. It is of interest to perform a detailed and large-scale study to investigate the effects on the calculated results due to these differences.

Recently, one of the authors developed a fully relativistic configuration-interaction code, i.e., the flexible atomic code (FAC), which integrated various atomic processes within a unified theoretical framework [17–19]. The atomic structure calculation in FAC is based on the relativistic configuration interaction method. The continuum processes, such as direct excitation and autoionization, are treated in the distorted-wave (DW) approximation. Special attention has been paid to the long-range contributions to the continuum-continuum radial integral by using a phase-amplitude method for the continuum wave functions. Systematic application of the factorization-interpolation method of Bar-Shalom [20] makes the code highly efficient for large scale calculations. FAC has been successfully used to obtain electron impact collision strengths without RE contributions for Ni-like tantalum [7,8]. In these calculations, to ensure the convergence of the collision strengths, large angular momentum contributions (the maximum partial waves up to 50) have been taken into account. Higher partial-wave contributions have been included using the Coulomb-Bethe approximation. One can find more details about FAC from Refs. [17–19] and the manual of the codes.

In this work, also using FAC, we will present a detailed and large-scale calculation on the resonant excitation rate coefficients from the ground level to the 106 fine-structure levels belonging to the $3l^{17}4l'$ ($l=0,1,2$; $l'=0,1,2,3$) configurations of Ni-like tantalum. Contributions through all possible Cu-like doubly excited states of $3l^{17}4l'n''l''$ and $3l^{17}5l'n''l''$ configurations associated with $\Delta n=1$ and $\Delta n=2$ core excitations are included explicitly up to $n''=15$. After being checked, the n''^{-3} scaling law is used to extrapolate the contributions from high Rydberg states with $n''>15$. Configuration interactions within the same complexes are taken into account. The effects of radiation damping and decays to autoionizing levels possibly followed by autoionzation cascades (DAC) are discussed. Large discrepancies are found from the comparison of the present RE rate coefficients with existing results. Due to the more detailed considerations in our calculations, the present results should be more reliable and accurate.

In Sec. II the theoretical methods are outlined. Section III is the major part of this paper. The calculations of level structure, Auger, and radiative rates are given in Sec. III A. The partial contributions from l'', n'', and each complexes series are discussed in Sec. III B, III C, and III D. The discussion of the radiation damping and DAC effects on RE rate coefficients is given in Sec. III E. The RE rate coefficients of Ta^{45+} are presented together with DE rates in Sec. III F. The present results are compared with those of Chen and Osterheld [14] in Sec. III G. Secion IV is a brief summary.

II. THEORETICAL METHOD

When an electron impacts a Ta^{45+} ion in the ground state, one M-shell electron can be excited while the incident electron is simultaneously captured to form a doubly excited state of Ta^{44+}. This process is known as dielectronic capture (DC) or resonant capture. The doubly excited states can subsequently Auger decay to the ground state, or the singly excited states of Ta^{45+}. The latter is resonance excitation (RE), which has the same end result as directly exciting one M-shell electron. The direct-excitation (DE) process for $3l$ ($l\leqslant 2$) to $4l$ ($l\leqslant 3$) transitions can be represented by

$$e^- + 3l^{18} \rightarrow 3l^{17}4l + e^-. \tag{1}$$

The notations $3l^{18}$, both $3l^{17}$ and $3l^{-1}$, represent M shell being fully filled and having a single hole in one of the $3s$, $3p$, or $3d$ subshells. The RE process with M-shell excitation can be described by

$$e^- + 3l^{18} \rightarrow 3l^{17}n'l'n''l'' \rightarrow 3l^{17}4l + e^- \tag{2}$$

or

$$3l^{17}n'l'n''l'' \rightarrow 3l^{17}n'l'n'''l''' + h\nu \rightarrow 3l^{17}4l + e^- + h\nu. \tag{3}$$

Equation (3) describes the RE contribution from DAC processes.

In the isolated resonance and independent-process approximation, and neglecting the profile of the resonances, one can obtain the DC strength using the detailed balance principle [21]

$$S_{ij}^{DC} = \frac{\pi^2\hbar^3}{m_e}\frac{g_j}{2g_iE_{ij}}A_{ji}^a\delta(E-E_{ij}), \tag{4}$$

where i and j represent the ground state of Ta^{45+} and an autoionizing doubly excited state of Ta^{44+}, respectively; E_{ij} and E are the resonance energy and incident electron energy; m_e is the mass of electron; g_i and g_j are the statistical weights of states i and j; A_{ji}^a is the Auger rate from j to i.

Assuming that the ion does not undergo inelastic collisions with electrons after capturing the free electron, the Cu-like ion in level j can either autoionize to form a Ni-like ion in level f or decay radiatively. The final state of the radiative decay can either be a level d below the first ionization limit k or a level j' above k. From j' the Cu-like ion can further decay radiatively or autoionize to level f if energetically allowed [i.e., the contributions from DAC as seen in Eq. (3)]. Therefore, considering all possible depletion processes from a given level j, the branching ratio for resonant excitation to level f through the level j is defined iteratively as

$$B_{jf}^{RE} = \frac{A_{jf}^a + \sum_{j'>k} A_{jj'}^r B_{j'f}^{RE}}{\sum_{d<k} A_{jd}^r + \sum_{j'>k} A_{jj'}^r + \sum_{f'} A_{jf'}^a}, \tag{5}$$

where ΣA_{jd}^r and $\Sigma A_{jj'}^r$ are total dipole transition rates from level j to levels d and j', respectively. $\Sigma A_{jf'}^a$ is the total autoionization rate from level j to all possible Ni-like levels f'. $B_{j'f}^{RE}$ is the RE branching ratio through level j' to level f, and is defined to be zero if j' to f transition is energetically forbidden. The inclusion of ΣA_{jd}^r in Eq. (5) can cause a significant reduction of RE rate coefficients, and including both $\Sigma A_{jj'}^r$ in the denominator and $\Sigma_{j'>k}A_{jj'}^r B_{j'f}^{RE}$ in the numerator

usually reduces RE rates. The above effects are referred to as radiation damping [13] and DAC effects. We will give a detailed discussion of their importance in Sec. III E.

By using Eqs. (4) and (5), and summing over all possible levels j, one can obtain the RE strength from i to f. In order to compare the calculated RE cross sections with experiments, the strengths should be convoluted with the energy distribution of incident electrons. Assuming a Maxwellian velocity distribution of the thermal plasma electrons, RE rate coefficients at temperature T from level i to f are given by

$$\alpha_{if}(kT) = \frac{(2\pi)^{3/2}\hbar^3}{(m_e kT)^{3/2}} \Sigma_j \frac{g_j}{2g_i} A^a_{ji} B^{RE}_{jf} \exp\left(-\frac{E_{ij}}{k_B T}\right). \quad (6)$$

III. THE CALCULATION OF RE RATE COEFFICIENTS FOR Ta^{45+}

A. Calculations of energy levels, radiative, and Auger rates

The energy levels for Ta^{45+} obtained with FAC have been reported by the study on the direct excitation and compared with other results [8]. To refer to the levels conveniently, we calculate again and list the energies of the 106 levels belonging to the $3l^{17}4l'$ configurations relative to the ground state in Table I. The levels are identified by their dominant components in the j-j coupled basis set. The electron correlations among all possible $3l^{18}$, $3l^{17}4l'$, and $3l^{17}5l'$ configurations are taken into account. Relativistic effects are fully considered using the Dirac Coulomb Hamiltonian. Higher-order QED effects are included with Breit interaction in the zero energy limit for the exchanged photon, and screened hydrogenic approximations for self-energy and vaccum polarization effects. Our results for the $3d^9 4l$ states agree well with Chen's [14] to within 0.5%.

As mentioned before, we explicitly include the RE contributions through Cu-like configurations $3l^{17}n'l'n''l''$ ($l=0,1,2$; $n'=4,5$; $l'=0,1,\ldots n'-1$; $n''\leqslant 15$, $l''\leqslant 8$). The total number of autoionizing levels within these configurations is about two hundred thousands. The configuration interactions within the same complexes are taken into account. For example, all possible configurations of $3l^{17}n'l'n''l''$ with given n' and n'' are included in one configuration interaction (CI) calculation to obtain the energy levels and wave functions.

Figure 1 shows the energy spread of the complexes series of Ta^{45+} and Ta^{44+} included in the present work. The calculation shows that most of the levels in $3s^2 3p^6 3d^9 4l' 4l''$ and low-lying levels in $3s^2 3p^5 3d^{10} 4l' 4l''$ doubly configurations are below the ionization limit of Cu-like Ta^{44+}, and the lowest excited level of Ni-like Ta^{45+}, i.e., the level No. 2 in Table I, is too high for many doubly excited states of Ta^{44+} to give RE contributions. The high-lying levels in $3s^2 3p^6 3d^9 4l' n''l''$ complex series are above No. 2 level only when $n''\geqslant 7$. For other complexes series, the energies become higher than the No. 2 level when $n''\geqslant 5$.

The spontaneous decay rates are calculated in the single multipole approximation [19]. In the present work, only $E1$ transitions are included. The total number of dipole transitions included is up to many 10^6. For the summation $\Sigma_{d<k} A^r_{jd}$ in Eq. (5), we take into account radiative rates of all possible resonant stabilizing transitions from level j to levels d in $3l^{18}n'l'$ or $3l^{18}n''l''$ configurations, and nonresonant stabilizing transitions from level j to levels d in low-lying $3l^{17}4l'4l''$ states (according to Refs. [22,23], these two kinds of transitions are referred to as RS and NRS). Both RS and NRS transitions account for the radiation damping effects on RE and give contributions to DR. For the summation $\Sigma_{j'>k} A^r_{jj'}$ in Eq. (5), as discussed in Ref. [22], the inclusion of all DAC transitions from level j to other lower autoionizing levels j' is computationally prohibitive for the higher complexes. The DAC effects were only considered for $3d^9 4l 4l'$ and $3d^9 4l 5l'$ in the study on DR [22]. But in the case of RE, as seen from Fig. 1, there are many autoionizing doubly excited states below the first excited level f'' of Ta^{45+}. Radiative transitions to these states will give no contribution to RE. Hence, the DAC transitions to levels below f'' should be taken into account as purely damping sources. Here, we consider as many DAC transitions as possible given our present computational ability. For $3l^{17}4l'n''l''$ complex series, all possible transitions to $3l^{17}4l'n'''l'''$ with $n'''\leqslant 10$ and possible $\Delta n=0$ transitions among M or N shells are taken into account. For $3l^{17}5l'n''l''$ complex series, we include all possible transitions to $3l^{17}5l'n'''l'''$ with $n'''\leqslant 6$ and $3l^{17}4l'''n''l''$, where both $n''l''$ Rydberg and $5l'$ core electrons are involved in the transitions.

The Auger rates are calculated in the first order perturbation theory [19]. For the summation $\Sigma A^a_{jf'}$ in Eq. (5), the Auger decays energetically allowed from the doubly excited states of Cu-like to Ni-like $3l^{18}$, $3l^{17}4l'$, and $3l^{17}5l'$ states are all taken into account. Due to the inclusion of configuration-interaction, there are some Auger decays involving three electrons which are forbidden when electron correlations are neglected. These Auger decays can also give RE contributions as shown in Sec. III D.

B. Partial contribution of complexes with orbital angular momentum l''

Autoionizing doubly excited configurations of $3l^{17}4l'n''l''$ and $3l^{17}5l'n''l''$ with $0\leqslant l''\leqslant 8$ are included in the present calculations. The contributions through the configurations with higher l'' values are neglected for all values of n''. The total RE rate coefficients, which are the sum of detailed RE rates for each singly excited states, through all possible configurations of $3l^{17}4l'15l''$ and $3l^{17}5l'15l''$ are plotted in Fig. 2 as functions of l''. It is clear that the contributions from configurations with $l''>8$ are expected to be negligible for both $n''=15$ complexes. The reason for this trend is the steep decrease of the Auger rates, A^a_{ji}, in Eq. (4) as l'' increases. For example, the sum of autoionization rates $\Sigma_j A^a_{ji}$ within all possible $3l^{17}4l'15l''$ configurations with $l''=4$ and $l''=8$ are 6.59×10^{13} s^{-1} and 1.57×10^{11} s^{-1}, respectively. The corresponding values for $3l^{17}5l'15l''$ with $l''=4$ and $l''=8$ are 1.82×10^{13} s^{-1} and 1.34×10^{10} s^{-1}. This conclusion is also found to be valid for all other complexes series. Thus the complete neglect of configurations with $l''>8$ is justified. It should be pointed out that the contributions from the con-

TABLE I. Energy-level definitions for Ni-like tantalum.

Index	State configuration	Energy (eV)	Index	State configuration	Energy (eV)
1	$3s^2 3p_{1/2}^2 3p_{3/2}^4 3d_{3/2}^4 3d_{5/2}^6 J=0$	0.0	55	$3s^2 3p_{1/2}^2 3p_{3/2}^4 3d_{3/2}^3 3d_{5/2}^6 4f_{7/2} J=5$	2078.9
2	$3s^2 3p_{1/2}^2 3p_{3/2}^4 3d_{3/2}^4 3d_{5/2}^5 4s J=3$	1502.6	56	$3s^2 3p_{1/2}^2 3p_{3/2}^4 3d_{3/2}^3 3d_{5/2}^6 4f_{5/2} J=3$	2079.4
3	$3s^2 3p_{1/2}^2 3p_{3/2}^4 3d_{3/2}^4 3d_{5/2}^5 4s J=2$	1504.5	57	$3s^2 3p_{1/2}^2 3p_{3/2}^4 3d_{3/2}^3 3d_{5/2}^6 4f_{7/2} J=3$	2082.0
4	$3s^2 3p_{1/2}^2 3p_{3/2}^4 3d_{3/2}^3 3d_{5/2}^6 4s J=1$	1564.9	58	$3s^2 3p_{1/2}^2 3p_{3/2}^4 3d_{3/2}^3 3d_{5/2}^6 4f_{7/2} J=4$	2083.3
5	$3s^2 3p_{1/2}^2 3p_{3/2}^4 3d_{3/2}^3 3d_{5/2}^6 4s J=2$	1566.1	59	$3s^2 3p_{1/2}^2 3p_{3/2}^4 3d_{3/2}^3 3d_{5/2}^6 4f_{5/2} J=1$	2099.8
6	$3s^2 3p_{1/2}^2 3p_{3/2}^4 3d_{3/2}^4 3d_{5/2}^5 4p_{1/2} J=2$	1596.7	60	$3s^2 3p_{1/2}^2 3p_{3/2}^3 3d_{3/2}^4 3d_{5/2}^6 4p_{3/2} J=3$	2134.0
7	$3s^2 3p_{1/2}^2 3p_{3/2}^4 3d_{3/2}^4 3d_{5/2}^5 4p_{1/2} J=3$	1597.9	61	$3s^2 3p_{1/2}^2 3p_{3/2}^3 3d_{3/2}^4 3d_{5/2}^6 4p_{3/2} J=1$	2134.1
8	$3s^2 3p_{1/2}^2 3p_{3/2}^4 3d_{3/2}^3 3d_{5/2}^6 4p_{1/2} J=2$	1659.0	62	$3s^2 3p_{1/2}^2 3p_{3/2}^3 3d_{3/2}^4 3d_{5/2}^6 4p_{3/2} J=2$	2139.2
9	$3s^2 3p_{1/2}^2 3p_{3/2}^4 3d_{3/2}^3 3d_{5/2}^6 4p_{1/2} J=1$	1662.4	63	$3s^2 3p_{1/2}^2 3p_{3/2}^3 3d_{3/2}^4 3d_{5/2}^6 4p_{3/2} J=0$	2157.8
10	$3s^2 3p_{1/2}^2 3p_{3/2}^4 3d_{3/2}^4 3d_{5/2}^5 4p_{3/2} J=4$	1692.5	64	$3s^2 3p_{1/2}^1 3p_{3/2}^4 3d_{3/2}^4 3d_{5/2}^6 4s J=0$	2231.2
11	$3s^2 3p_{1/2}^2 3p_{3/2}^4 3d_{3/2}^4 3d_{5/2}^5 4p_{3/2} J=2$	1694.5	65	$3s^2 3p_{1/2}^1 3p_{3/2}^4 3d_{3/2}^4 3d_{5/2}^6 4s J=1$	2233.5
12	$3s^2 3p_{1/2}^2 3p_{3/2}^4 3d_{3/2}^4 3d_{5/2}^5 4p_{3/2} J=1$	1695.7	66	$3s^2 3p_{1/2}^2 3p_{3/2}^3 3d_{3/2}^4 3d_{5/2}^6 4d_{3/2} J=0$	2275.5
13	$3s^2 3p_{1/2}^2 3p_{3/2}^4 3d_{3/2}^4 3d_{5/2}^5 4p_{3/2} J=3$	1697.7	67	$3s^2 3p_{1/2}^2 3p_{3/2}^3 3d_{3/2}^4 3d_{5/2}^6 4d_{3/2} J=1$	2278.9
14	$3s^2 3p_{1/2}^2 3p_{3/2}^4 3d_{3/2}^3 3d_{5/2}^6 4p_{3/2} J=0$	1751.5	68	$3s^2 3p_{1/2}^2 3p_{3/2}^3 3d_{3/2}^4 3d_{5/2}^6 4d_{3/2} J=3$	2279.7
15	$3s^2 3p_{1/2}^2 3p_{3/2}^4 3d_{3/2}^3 3d_{5/2}^6 4p_{3/2} J=1$	1756.1	69	$3s^2 3p_{1/2}^2 3p_{3/2}^3 3d_{3/2}^4 3d_{5/2}^6 4d_{3/2} J=2$	2282.8
16	$3s^2 3p_{1/2}^2 3p_{3/2}^4 3d_{3/2}^3 3d_{5/2}^6 4p_{3/2} J=3$	1756.3	70	$3s^2 3p_{1/2}^2 3p_{3/2}^3 3d_{3/2}^4 3d_{5/2}^6 4d_{5/2} J=4$	2299.1
17	$3s^2 3p_{1/2}^2 3p_{3/2}^4 3d_{3/2}^3 3d_{5/2}^6 4p_{3/2} J=2$	1759.0	71	$3s^2 3p_{1/2}^2 3p_{3/2}^3 3d_{3/2}^4 3d_{5/2}^6 4d_{5/2} J=2$	2301.1
18	$3s^2 3p_{1/2}^2 3p_{3/2}^4 3d_{3/2}^4 3d_{5/2}^5 4d_{3/2} J=1$	1832.8	72	$3s^2 3p_{1/2}^2 3p_{3/2}^3 3d_{3/2}^4 3d_{5/2}^6 4d_{5/2} J=1$	2301.7
19	$3s^2 3p_{1/2}^2 3p_{3/2}^4 3d_{3/2}^4 3d_{5/2}^5 4d_{3/2} J=4$	1837.8	73	$3s^2 3p_{1/2}^2 3p_{3/2}^3 3d_{3/2}^4 3d_{5/2}^6 4d_{5/2} J=3$	2304.3
20	$3s^2 3p_{1/2}^2 3p_{3/2}^4 3d_{3/2}^4 3d_{5/2}^5 4d_{3/2} J=2$	1839.2	74	$3s^2 3p_{1/2}^1 3p_{3/2}^4 3d_{3/2}^4 3d_{5/2}^6 4p_{1/2} J=1$	2326.2
21	$3s^2 3p_{1/2}^2 3p_{3/2}^4 3d_{3/2}^4 3d_{5/2}^5 4d_{3/2} J=3$	1841.5	75	$3s^2 3p_{1/2}^1 3p_{3/2}^4 3d_{3/2}^4 3d_{5/2}^6 4p_{1/2} J=0$	2341.7
22	$3s^2 3p_{1/2}^2 3p_{3/2}^4 3d_{3/2}^4 3d_{5/2}^5 4d_{5/2} J=1$	1855.3	76	$3s^2 3p_{1/2}^1 3p_{3/2}^4 3d_{3/2}^4 3d_{5/2}^6 4p_{3/2} J=1$	2420.9
23	$3s^2 3p_{1/2}^2 3p_{3/2}^4 3d_{3/2}^4 3d_{5/2}^5 4d_{5/2} J=5$	1856.9	77	$3s^2 3p_{1/2}^1 3p_{3/2}^4 3d_{3/2}^4 3d_{5/2}^6 4p_{3/2} J=2$	2424.2
24	$3s^2 3p_{1/2}^2 3p_{3/2}^4 3d_{3/2}^4 3d_{5/2}^5 4d_{5/2} J=3$	1860.8	78	$3s^2 3p_{1/2}^2 3p_{3/2}^3 3d_{3/2}^4 3d_{5/2}^6 4f_{5/2} J=1$	2446.3
25	$3s^2 3p_{1/2}^2 3p_{3/2}^4 3d_{3/2}^4 3d_{5/2}^5 4d_{5/2} J=2$	1862.0	79	$3s^2 3p_{1/2}^2 3p_{3/2}^3 3d_{3/2}^4 3d_{5/2}^6 4f_{5/2} J=2$	2451.0
26	$3s^2 3p_{1/2}^2 3p_{3/2}^4 3d_{3/2}^4 3d_{5/2}^5 4d_{5/2} J=4$	1862.7	80	$3s^2 3p_{1/2}^2 3p_{3/2}^3 3d_{3/2}^4 3d_{5/2}^6 4f_{5/2} J=4$	2452.2
27	$3s^2 3p_{1/2}^2 3p_{3/2}^4 3d_{3/2}^4 3d_{5/2}^5 4d_{5/2} J=0$	1876.1	81	$3s^2 3p_{1/2}^2 3p_{3/2}^3 3d_{3/2}^4 3d_{5/2}^6 4f_{7/2} J=5$	2455.0
28	$3s^2 3p_{1/2}^2 3p_{3/2}^4 3d_{3/2}^3 3d_{5/2}^6 4d_{3/2} J=1$	1899.1	82	$3s^2 3p_{1/2}^2 3p_{3/2}^3 3d_{3/2}^4 3d_{5/2}^6 4f_{5/2} J=3$	2455.9
29	$3s^2 3p_{1/2}^2 3p_{3/2}^4 3d_{3/2}^3 3d_{5/2}^6 4d_{3/2} J=3$	1899.5	83	$3s^2 3p_{1/2}^2 3p_{3/2}^3 3d_{3/2}^4 3d_{5/2}^6 4f_{7/2} J=3$	2459.0
30	$3s^2 3p_{1/2}^2 3p_{3/2}^4 3d_{3/2}^3 3d_{5/2}^6 4d_{3/2} J=2$	1905.2	84	$3s^2 3p_{1/2}^2 3p_{3/2}^3 3d_{3/2}^4 3d_{5/2}^6 4f_{7/2} J=4$	2462.8
31	$3s^2 3p_{1/2}^2 3p_{3/2}^4 3d_{3/2}^3 3d_{5/2}^6 4d_{5/2} J=1$	1917.7	85	$3s^2 3p_{1/2}^2 3p_{3/2}^3 3d_{3/2}^4 3d_{5/2}^6 4f_{7/2} J=2$	2466.6
32	$3s^2 3p_{1/2}^2 3p_{3/2}^4 3d_{3/2}^3 3d_{5/2}^6 4d_{5/2} J=4$	1920.8	86	$3s^1 3p_{1/2}^2 3p_{3/2}^4 3d_{3/2}^4 3d_{5/2}^6 4s J=1$	2469.3
33	$3s^2 3p_{1/2}^2 3p_{3/2}^4 3d_{3/2}^3 3d_{5/2}^6 4d_{5/2} J=2$	1922.6	87	$3s^1 3p_{1/2}^2 3p_{3/2}^4 3d_{3/2}^4 3d_{5/2}^6 4s J=0$	2477.7
34	$3s^2 3p_{1/2}^2 3p_{3/2}^4 3d_{3/2}^3 3d_{5/2}^6 4d_{5/2} J=3$	1924.4	88	$3s^1 3p_{1/2}^2 3p_{3/2}^4 3d_{3/2}^4 3d_{5/2}^6 4p_{1/2} J=1$	2555.9
35	$3s^2 3p_{1/2}^2 3p_{3/2}^3 3d_{3/2}^4 3d_{5/2}^6 4s J=2$	1944.0	89	$3s^1 3p_{1/2}^2 3p_{3/2}^4 3d_{3/2}^4 3d_{5/2}^6 4p_{1/2} J=0$	2561.3
36	$3s^2 3p_{1/2}^2 3p_{3/2}^4 3d_{3/2}^3 3d_{5/2}^6 4d_{3/2} J=0$	1944.0	90	$3s^2 3p_{1/2}^1 3p_{3/2}^4 3d_{3/2}^4 3d_{5/2}^6 4d_{3/2} J=2$	2570.8
37	$3s^2 3p_{1/2}^2 3p_{3/2}^3 3d_{3/2}^4 3d_{5/2}^6 4s J=1$	1947.3	91	$3s^2 3p_{1/2}^1 3p_{3/2}^4 3d_{3/2}^4 3d_{5/2}^6 4d_{3/2} J=1$	2576.8
38	$3s^2 3p_{1/2}^2 3p_{3/2}^4 3d_{3/2}^4 3d_{5/2}^5 4f_{5/2} J=0$	2003.4	92	$3s^2 3p_{1/2}^1 3p_{3/2}^4 3d_{3/2}^4 3d_{5/2}^6 4d_{5/2} J=2$	2587.5
39	$3s^2 3p_{1/2}^2 3p_{3/2}^4 3d_{3/2}^4 3d_{5/2}^5 4f_{5/2} J=1$	2006.3	93	$3s^2 3p_{1/2}^1 3p_{3/2}^4 3d_{3/2}^4 3d_{5/2}^6 4d_{5/2} J=3$	2589.0
40	$3s^2 3p_{1/2}^2 3p_{3/2}^4 3d_{3/2}^4 3d_{5/2}^5 4f_{5/2} J=5$	2010.4	94	$3s^1 3p_{1/2}^2 3p_{3/2}^4 3d_{3/2}^4 3d_{5/2}^6 4p_{3/2} J=2$	2658.9
41	$3s^2 3p_{1/2}^2 3p_{3/2}^4 3d_{3/2}^4 3d_{5/2}^5 4f_{5/2} J=2$	2011.1	95	$3s^1 3p_{1/2}^2 3p_{3/2}^4 3d_{3/2}^4 3d_{5/2}^6 4p_{3/2} J=1$	2660.6
42	$3s^2 3p_{1/2}^2 3p_{3/2}^4 3d_{3/2}^4 3d_{5/2}^5 4f_{7/2} J=6$	2014.1	96	$3s^2 3p_{1/2}^1 3p_{3/2}^4 3d_{3/2}^4 3d_{5/2}^6 4f_{5/2} J=3$	2740.6
43	$3s^2 3p_{1/2}^2 3p_{3/2}^4 3d_{3/2}^4 3d_{5/2}^5 4f_{5/2} J=3$	2014.3	97	$3s^2 3p_{1/2}^1 3p_{3/2}^4 3d_{3/2}^4 3d_{5/2}^6 4f_{7/2} J=3$	2744.4
44	$3s^2 3p_{1/2}^2 3p_{3/2}^4 3d_{3/2}^4 3d_{5/2}^5 4f_{5/2} J=4$	2015.5	98	$3s^2 3p_{1/2}^1 3p_{3/2}^4 3d_{3/2}^4 3d_{5/2}^6 4f_{5/2} J=2$	2745.4
45	$3s^2 3p_{1/2}^2 3p_{3/2}^4 3d_{3/2}^4 3d_{5/2}^5 4f_{7/2} J=2$	2015.8	99	$3s^2 3p_{1/2}^1 3p_{3/2}^4 3d_{3/2}^4 3d_{5/2}^6 4f_{7/2} J=4$	2747.5
46	$3s^2 3p_{1/2}^2 3p_{3/2}^4 3d_{3/2}^4 3d_{5/2}^5 4f_{7/2} J=4$	2019.8	100	$3s^1 3p_{1/2}^2 3p_{3/2}^4 3d_{3/2}^4 3d_{5/2}^6 4d_{3/2} J=1$	2802.5
47	$3s^2 3p_{1/2}^2 3p_{3/2}^4 3d_{3/2}^4 3d_{5/2}^5 4f_{7/2} J=5$	2021.2	101	$3s^1 3p_{1/2}^2 3p_{3/2}^4 3d_{3/2}^4 3d_{5/2}^6 4d_{3/2} J=2$	2803.9
48	$3s^2 3p_{1/2}^2 3p_{3/2}^4 3d_{3/2}^4 3d_{5/2}^5 4f_{7/2} J=3$	2021.9	102	$3s^1 3p_{1/2}^2 3p_{3/2}^4 3d_{3/2}^4 3d_{5/2}^6 4d_{5/2} J=3$	2823.5

TABLE I. (*Continued.*)

Index	State configuration	Energy (eV)	Index	State configuration	Energy (eV)
49	$3s^23p_{1/2}^2 3p_{3/2}^4 3d_{3/2}^4 3d_{5/2}^5 4f_{7/2} J=1$	2034.3	103	$3s^1 3p_{1/2}^2 3p_{3/2}^4 3d_{3/2}^4 3d_{5/2}^6 4d_{5/2} J=2$	2824.3
50	$3s^23p_{1/2}^2 3p_{3/2}^3 3d_{3/2}^4 3d_{5/2}^6 4p_{1/2} J=1$	2038.6	104	$3s^1 3p_{1/2}^2 3p_{3/2}^4 3d_{3/2}^4 3d_{5/2}^6 4f_{5/2} J=2$	2973.8
51	$3s^23p_{1/2}^2 3p_{3/2}^3 3d_{3/2}^4 3d_{5/2}^6 4p_{1/2} J=2$	2039.6	105	$3s^1 3p_{1/2}^2 3p_{3/2}^4 3d_{3/2}^4 3d_{5/2}^6 4f_{5/2} J=3$	2975.1
52	$3s^23p_{1/2}^2 3p_{3/2}^4 3d_{3/2}^3 3d_{5/2}^6 4f_{5/2} J=4$	2072.4	106	$3s^1 3p_{1/2}^2 3p_{3/2}^4 3d_{3/2}^4 3d_{5/2}^6 4f_{7/2} J=4$	2979.0
53	$3s^23p_{1/2}^2 3p_{3/2}^4 3d_{3/2}^3 3d_{5/2}^6 4f_{5/2} J=2$	2073.7	107	$3s^1 3p_{1/2}^2 3p_{3/2}^4 3d_{3/2}^4 3d_{5/2}^6 4f_{7/2} J=3$	2983.7
54	$3s^23p_{1/2}^2 3p_{3/2}^4 3d_{3/2}^3 3d_{5/2}^6 4f_{7/2} J=2$	2076.9			

figurations with $5 \leqslant l'' \leqslant 8$ accounts for about 15% of the total RE rate coefficients.

C. Partial contribution of complexes with principal quantum number n'' and extrapolation

Autoionizing doubly excited configurations of $3l^{17}4l'n''l''$ and $3l^{17}5l'n''l''$ associated with possible $\Delta n=1$ and $\Delta n=2$ core excitations are calculated explicitly up to $n''=15$. In order to estimate the contributions of higher complexes ($n''>15$) in each series, the n''^{-3} scaling law extrapolation method first proposed by Hahn [21] has been used. This scaling law is based on the fact that the Auger and radiative rates scale as n''^{-3} for high enough values of n''. Denoting by n_s the lowest n'' value above which $\alpha_{if}(n'')$ scales accurately enough as n''^{-3}, one can write the total RE rate coefficients from level i to level f as

$$\alpha_{if}(T) = \sum_{n'' \leqslant n_s} \alpha(T,n'') + \sum_{n''=n_s+1}^{\infty} \left(\frac{n''}{n_s}\right)^{-3} \alpha(T,n_s). \qquad (7)$$

As mentioned before, n_s was chosen to be 9 in Ref. [14], and 12 for $3d^94l'n''l''$ and 10 for $3p^54l'n''l''$ complexes series in Ref. [15]. In the present work, we find $n_s=15$ seems to be a more appropriate choice.

Figure 3(a) shows the n'' dependence of partial RE rate coefficients to the energy level No. 2 at an electron temperature of 1200 eV, around which the total RE rates peak. It can be seen that in the range $9 \leqslant n'' < 14$ there are irregularities in the behavior of the partial rate coefficients for resonances associated with all six core excitations. We find that sometimes the partial RE rate coefficients decrease more slowly than the n''^{-3} relation or even increase as n'' increases. This is due to the gradual openning of new effective RE channels as more and more energy levels in each complex series rise above the level No. 2. On the other hand, the rate coefficients may decrease more steeply than n''^{-3} due to the competition with other possible autoionizing channels. These additional autoionizing channels gradually open because levels in higher n'' complexes become energetically allowed to decay into more high-lying singly excited levels other than the level No. 2.

The partial RE rate coefficients at 1200 eV through the $3d^94l'n''l''$ complex series and the detailed contributions through $3d \rightarrow 4f$, $3d \rightarrow 4d$, and $3d \rightarrow 4p$ core excitations are plotted in Fig. 3(b) as functions of n''. The levels in $3d^94l'n''l''$ configurations can reach level No. 2 via $4s-4l'n''l''$ Coster-Kronig transitions [24]. The partial RE rate

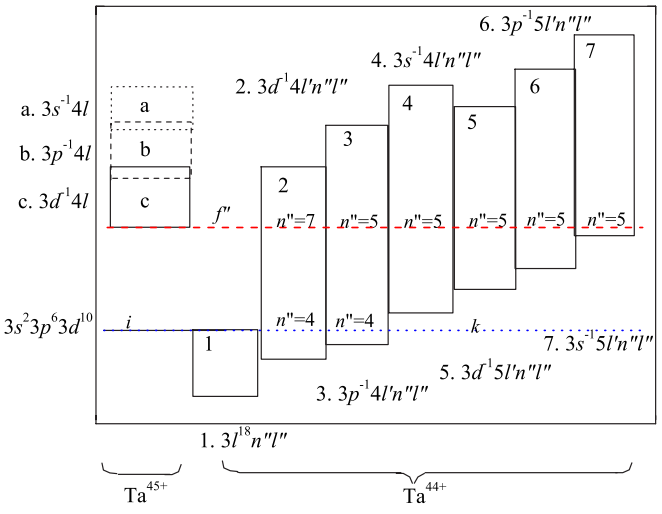

FIG. 1. (Color online) Energy scheme of Ni-like tantalum and Cu-like tantalum. k represents the ionization limit of Ta^{44+}. f'' represents the lowest excited level of Ta^{45+}. The equations, such as $n''=7$ and $n''=4$ in the $3d^{-1}4l'n''l''$ complex series box, represent corresponding complexes in which the high- and low-lying levels are above f'' and below k, respectively.

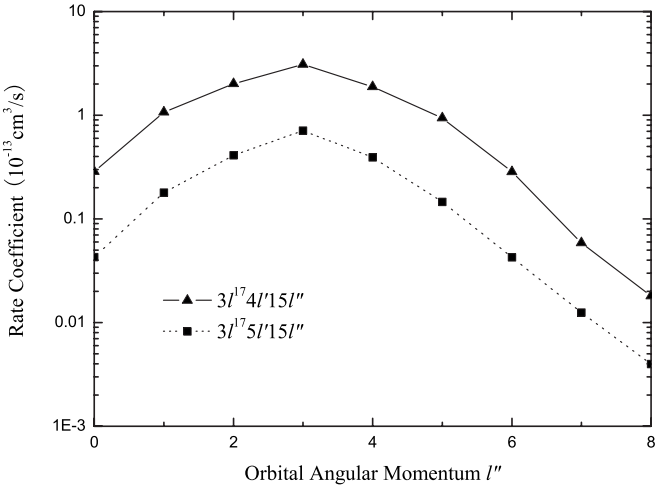

FIG. 2. Partial RE rate coefficients through the configurations of $3l^{17}4l'15l''$ (triangles) and $3l^{17}5l'15l''$ (squares) as functions of the orbital angular momentum l'', at an electron temperature of 1200 eV. The lines between the calculated values are plotted just to guide the eye.

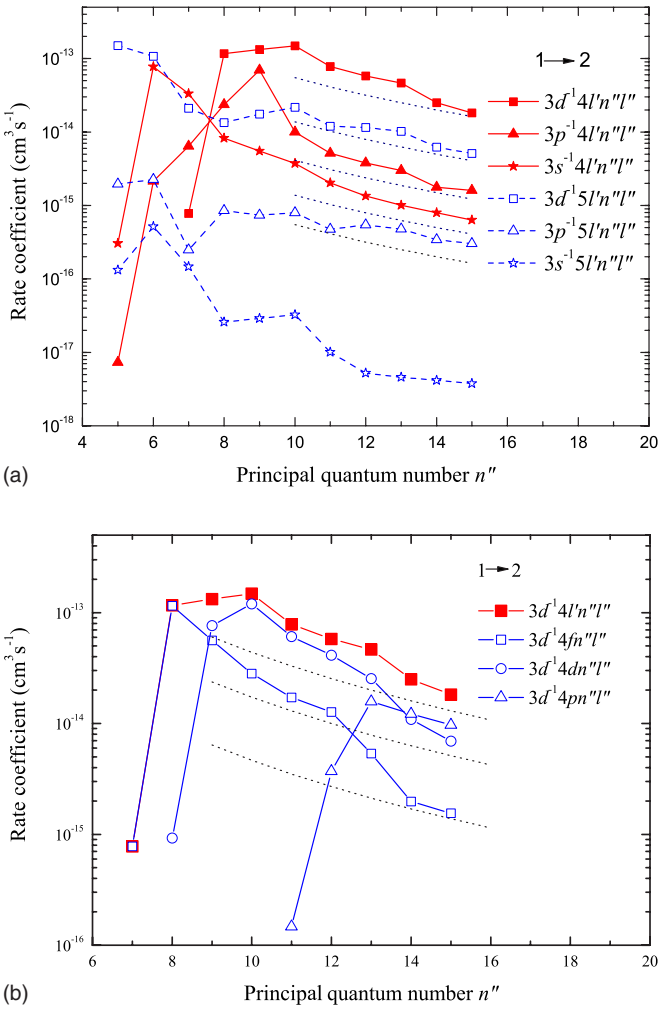

FIG. 3. (Color online) Partial RE rate coefficients through each core excitations to the energy level No. 2 as functions of n'', at an electron temperature 1200 eV. The lines between the calculated values are plotted just to guide the eye. The dotted curves indicate the n''^{-3} grid as reference for the scaling of the partial rate coefficients.

coefficients through $3d^94l'n''l''$ complex series increase in the range $8 \leqslant n'' \leqslant 10$ due to the gradual openning of $4s-4f_{7/2,5/2}8l''$, $4s-4d_{5/2}9l''$, and $4s-4d_{3/2}10l''$ Coster-Kronig transitions. The detailed RE contributions from $3d^94fn''l''$ $(8 \leqslant n'' \leqslant 14)$ and $3d^94dn''l''$ $(10 \leqslant n'' \leqslant 15)$ decrease more steeply than n''^{-3} because the $4p-4fn''l''$, $4d-4fn''l''$, and $4p-4dn''l''$ Coster-Kronig transitions open gradually with increasing n'', which redistribute the capture strengths to RE of more highly excited levels. The detailed RE contributions from $3d^94pn''l''$ with $13 \leqslant n'' \leqslant 15$ begin to follow the n''^{-3} scaling law because for these n'' values only the $4s-4pn''l''$ Coster-Kronig transitions are energetically allowed. It should be pointed out that the super Coster-Kronig transitions [25], such as $4s-4sn''l''$, $4p-4pn''l''$, $4d-4dn''l''$, and $4f-4fn''l''$, are almost all energetically forbidden for $n'' \leqslant 15$. When n'' is high enough, these autoionization processes can also take place and affect the RE rate coefficients, but this is beyond the scope of the present work.

Although there are irregularities at intermediate values of n'' as mentioned above, it can still be seen from Fig. 3(a) that the scaling of the partial contributions with $n'' \geqslant 14$ starts to follow approximately the n''^{-3} law with an uncertainty of about 5%. This conclusion is found to be valid for resonant excitation into other singly excited states as well. Hence, we can use the n''^{-3} scaling law [see Eq. (7)] to reliably evaluate the contributions from complexes with $n'' > 15$. The sum of extrapolated contributions are found to be at most 35% of the total RE rate coefficients for all transitions from the ground state to the 106 levels belonging to the $3l^{17}4l'$ configurations of Ni-like Ta^{45+} ion. The errors introduced by the extrapolation are estimated to be about 5% of the total RE rate coefficients. The extrapolations starting from lower n'', as were done in previous work, would introduce larger uncertainties into the total rates.

D. Partial contribution of each complexes series

Autoionizing doubly excited configurations in the six complexes series, i.e., (a) $3s^23p^63d^94l'n''l''$, (b) $3s^23p^53d^{10}4l'n''l''$, (c) $3s3p^63d^{10}4l'n''l''$, (d) $3s^23p^63d^95l'n''l''$, (e) $3s^23p^53d^{10}5l'n''l''$, and (f) $3s3p^63d^{10}5l'n''l''$, are included in the present calculation. The $3l^{17}4l'n''l''$ configurations can autoionize into the singly excited states $3l^{17}4l$ via $4l-4l'n''l''$ and $3l'-3ln''l''$ Coster-Kronig transitions. For example, the resonant levels in $3s3p^63d^{10}4l'n''l''$ configurations can reach the levels in $3d^94l'$, $3p^54l'$, and $3s4l$ via $3s-3dn''l''$, $3s-3pn''l''$, and $4l-4l'n''l''$ Coster-Kronig transitions. The configurations $3l^{17}5l'n''l''$ can autoionize into the levels in $3l^{17}4l$ through $\Delta n=1$ Auger pathways.

In Table II, the RE rate coefficients to energy levels Nos. 2, 59, 35, 99, 86, and 107 are listed at kT_e=400 eV, 1200 eV, and 2500 eV along with the partial contributions of the six complexes series. The above six levels are the lowest and highest levels of the singly excited configurations $3d^94l$, $3p^54l$, and $3s4l$ (see Table I). Some conclusions can be drawn from Table II. For levels in the $3d^94l$ configurations, the contributions from complexes series (a), (b), (c), and (d) accounts for most of the RE rate coefficients. Complex series (a) mainly contributes to the low-lying levels of $3d^94l$, while the contributions from (b) and (d) are predominant for high-lying levels. For the $3p^54l$ levels, the RE rate coefficients mainly come from complexes series (b), (c), and (e). The contributions from (b) and (e) are dominant for low-lying $3p^54l$ levels while (c) and (e) dominate the rates for high-lying $3p^54l$ levels. Complexes series (c) and (f) dominate the RE rate coefficients to the levels of $3s4l$ configurations. The contributions from (c) are significant only for the low-lying $3s4l$ levels. From above discussions, one may conclude that the close-coupling expansions involved in previous R matrix calculations [9–13] have not covered all dominant resonances, especially for transitions to high-lying singly excited states, because the contributions from $3l^{17}5l'n''l''$ complex are almost all neglected in these R-matrix calculations [9–13]. It can also be seen from Table II that the RE contributions from $4l-4l'n''l''$ Coster-Kronig transitions for individual singly excited level are larger at lower temperatures, and the contributions from $\Delta n=1$ Auger transitions become larger at higher temperature. This is obviously due to the

TABLE II. RE rate coefficients in 10^{-13} cm^3 s^{-1} for the selected six levels and the percentage contributions of the six complexes series (see text) to the total rates.

Temperature (eV)	Excited levels	Rate coefficients	Complexes series (%)					
			(a)	(b)	(c)	(d)	(e)	(f)
400	2	4.50	58.6	9.8	8.6	22.7	0.2	0.0
	59	0.741	0.0	44.0	3.2	52.6	0.1	0.0
	35	0.518	0.0	45.2	8.1	1.7	46.3	0.4
	99	0.013	0.0	0.0	57.0	0.0	42.1	0.9
	86	0.036	0.0	0.8	34.7	0.1	3.0	61.4
	107	0.004	0.0	0.0	0.0	0.0	0.9	99.1
1200	2	14.5	51.8	9.5	9.5	28.4	0.8	0.1
	59	6.51	0.0	43.6	3.2	52.8	0.3	0.0
	35	3.33	0.0	40.4	9.0	1.6	49.7	0.9
	99	0.318	0.0	0.0	50.4	0.0	47.7	1.9
	86	0.556	0.0	0.7	31.6	0.1	3.0	64.6
	107	0.171	0.0	0.0	0.0	0.0	0.7	99.2
2500	2	10.3	48.9	9.3	9.7	30.9	1.1	0.1
	59	5.92	0.0	43.4	3.2	52.9	0.4	0.1
	35	2.81	0.0	38.6	9.1	0.2	51.1	1.1
	99	0.375	0.0	0.0	48.3	0.0	49.3	2.4
	86	0.591	0.0	0.7	30.3	0.1	3.0	65.9
	107	0.228	0.0	0.0	0.0	0.0	0.6	99.3

lower and higher resonant energies associated with $\Delta n=1$ and $\Delta n=2$ core excitations in the initial dielectronic capture. In addition, it can be seen from Table II that the RE contributions arising from the inclusion of configuration interaction are about several percents of the total RE rate coefficients. For example, the percentage RE contributions to energy level No. 86 (i.e., $3s3p^6 3d^{10}4s$ $J=1$) through $3s^2 3p^5 3d^{10}5l'n''l''$ complex series are about 3.0%.

E. Effects of radiative damping and DAC

Disregarding the decays of doubly excited states $3l^{17}4l'n''l''$ and $3l^{17}5l'n''l''$ to autoionizing levels (i.e., the DAC transitions) leads to the following approximate expression for the RE branching ratio instead of Eq. (5):

$$B_{jf}^{\mathrm{RE}} \approx \frac{A_{jf}^a}{\sum_{d<k} A_{jd}^r + \sum_{f'} A_{jf'}^a}, \tag{8}$$

Even the RS and NRS transition rates, i.e., the sum of A_{jd}^r, can be neglected comparing to the total Auger rates in some cases as shown in Ref. [13]. This leads to the further approximation for the RE branching ratio,

$$B_{jf}^{\mathrm{RE}} \approx \frac{A_{jf}^a}{\sum_{f'} A_{jf'}^a}, \tag{9}$$

The RE rate coefficients calculated using Eqs. (5), (8), and (9) for the branching ratios, referred to here as *ratesA*, *ratesB*, and *ratesC*, will differ from each other. Following Ref. [13], *ratesB* and *ratesC* are also known as the radiatively damped and undamped RE rate coefficients.

The three sets of RE rate coefficients to energy levels Nos. 2, 59, 35, 99, 86, and 107 are listed in Table III at $kT=400$, 1200, and 2500 eV. It can be seen that radiative decays reduce significantly the RE rates for low-lying singly excited states while the reductions are negligible for high-lying states (see the differences between *ratesB* and *ratesC*). An overall comparison of the damped and undamped RE rate coefficients at $kT=1200$ eV to the 106 levels of $3l^{-1}4l'$ configurations shows that the percentage differences are larger than 100% for RE transitions to energy levels Nos. 22, 27, 28, 36, and 59, which all belong to the $3d^9 4l'$ configurations. The effect of damping on the resonant excitation to the level No. 28, i.e., $3d_{3/2}^3 3d_{5/2}^6 4d_{3/2}$ $J=1$, is the largest of all transitions from the ground state and its RE rate coefficients are reduced by nearly a factor of 4. The percentage differences are between 10% and 100% for the other 51 transitions, most of which are towards the levels in the $3d^9 4l'$ configurations. The differences are less than 10% for the remaining 50 transitions, most of which are to levels in the $3p^5 4l'$ and $3s4l'$ configurations. The significant damping effects on the RE rate coefficients to levels in the $3d^9 4l'$ configurations arise from the fact that the doubly excited states of $3d^9 4fn''l''$ and $3d^9 5fn''l''$ configurations, which are found to dominate the RE rate coefficents, can decay to nonautoionizing levels of Cu-like Ta^{44+} via strong $4f \rightarrow 3d$ and $5f \rightarrow 3d$ dipole transitions. The damping effects for levels in the $3p^5 4l'$ and $3s4l'$ configurations are negligible due to the lack of

TABLE III. RE rate coefficients (in $cm^3\ s^{-1}$) calculated in three different approximations at $kT=400$, 1200, and 2500 eV for selected six levels. The RE rate coefficients referred to as *ratesA*, *ratesB*, and *ratesC* are obtained by using Eqs. (5), (8), and (9) to calculate the RE branching ratios.

kT (eV)		Excited levels (eV)					
		2	59	35	99	86	107
400	*ratesA*	4.50×10^{-13}	7.41×10^{-14}	5.18×10^{-14}	1.32×10^{-15}	3.58×10^{-15}	4.40×10^{-16}
	ratesB	6.34×10^{-13}	8.80×10^{-14}	8.83×10^{-14}	1.47×10^{-15}	6.51×10^{-15}	5.57×10^{-16}
	ratesC	8.38×10^{-13}	1.68×10^{-13}	1.00×10^{-13}	1.48×10^{-15}	6.62×10^{-15}	5.58×10^{-16}
1200	*ratesA*	1.45×10^{-12}	6.51×10^{-13}	3.33×10^{-13}	3.18×10^{-14}	5.56×10^{-14}	1.71×10^{-14}
	ratesB	1.88×10^{-12}	7.83×10^{-13}	5.29×10^{-13}	3.62×10^{-14}	9.20×10^{-14}	2.20×10^{-14}
	ratesC	2.46×10^{-12}	1.61×10^{-12}	5.94×10^{-13}	3.64×10^{-14}	9.36×10^{-14}	2.20×10^{-14}
2500	*ratesA*	1.03×10^{-12}	5.92×10^{-13}	2.81×10^{-13}	3.75×10^{-14}	5.91×10^{-14}	2.28×10^{-14}
	ratesB	1.29×10^{-12}	7.13×10^{-13}	4.34×10^{-13}	4.29×10^{-14}	9.44×10^{-14}	2.95×10^{-14}
	ratesC	1.68×10^{-12}	1.50×10^{-12}	4.86×10^{-13}	4.31×10^{-14}	9.61×10^{-14}	2.95×10^{-14}

strong dipole transitions to nonautoionizing states from the $(3p,3s)^{-1}4fn''l''$ and $(3p,3s)^{-1}5fn''l''$ configurations, which are found to dominate the RE contributions.

It can also be seen from Table III that DAC transitions reduce significantly the RE rate coefficients for all six levels (see the differences between *ratesA* and *ratesB*). The overall comparison of the RE rate coefficients, at $kT=1200$ eV, with and without considering DAC effects for the 106 transitions shows that the percentage differences are larger than 50% for energy levels No. 35, 64, and 86. The corresponding values are 59%, 57%, and 66%, respectively. The percentage differences are between 10% and 50% for 101 transitions, and are about 8% for the remaining two transitions into energy levels Nos. 12 and 95. The reason for significant reductions caused by the inclusion of DAC transitions has been mentioned in Sec. III A. First, there are many low-lying autoionizing levels between the first ionization limit of Ta^{44+} and the first singly excited level of Ta^{45+}. Hence, the strength decaying radiatively into these states from the resonant states are fully lost. The possible $3l^{-1}5l'n''l''$ configurations dominating the RE rates all have strong $n=5\rightarrow4$ and $n''\rightarrow4$ dipole transitions to the low-lying autoionizing levels (it should be pointed out that the lowest value of n'' is also 5). Finally, these DAC transition rates from the resonant states are comparable to the sum of total Auger rates and radiative transition rates to the bound states of Ta^{44+}.

F. DE and RE rate coefficients

The electron impact collision strengths of Ni-like Ta^{45+} ion have been calculated by employing FAC without consideration of resonance contributions [7,8]. In order to give a comparison between the DE and present RE rate coefficients, we also calculate the DE rate coefficients using the background collision strengths from FAC. We perform the calculations of collision strengths at 20 energies of the scattered electron from 10 to 25 000 eV. The electron correlations among all possible $3l^{18}$, $3l^{17}4l'$, and $3l^{17}5l'$ configurations are taken into account. In Table IV, the calculated direct and resonant excitation rate coefficients for Ta^{45+} from the ground state to 106 singly excited states in the $3l^{17}4l'$ configurations are given for electron temperatures $400\leqslant kT\leqslant2500$ eV. The following conclusions can be drawn from Table IV:

(1) For electron temperatures $kT<2500$ eV, RE are as important as DE processes for many transitions. RE rates coefficients peak around $kT=1200$ eV for the low-lying singly excited levels. For high-lying levels, the temperatures where the peaks locate increase. For example, the RE rate coefficients peak around $kT=2500$ eV for the level No. 107. The direct-excitation rates peak at much higher temperatures. As temperature increases, the importance of the resonances slowly diminishes.

(2) At the temperature of 400 eV, the ratios of RE to DE rate coefficients are larger than 5.0 for 8 of the 106 transitions, i.e., the transitions into energy levels Nos. 2, 4, 6, 8, 9, 11, 15, and 17. The largest ratio is 9.1 for the level No. 4. It should be pointed out that the ratios will be larger at lower-temperatures for each transition. The above eight transitions are all dipole-forbidden excitations except for the two transitions to energy levels Nos. 9 and 15. We find that there are large low-energy resonance contributions for levels Nos. 9 and 15, and the ratios for these two transitions decrease fast as the temperature increases. At $kT=5000$ eV, they are both less than 0.5 while the ratios for the other six transitions are still larger than 1.5. In addition, the ratios are between 1.0 and 5.0 for other 54 of the 106 transitions at $kT=400$ eV.

(3) At the temperature of 1200 eV, the ratios are larger than 1.0 for 34 transitions. The largest one is 5.4 for the level No. 4. For 62 transitions the ratios are between 0.1 and 1.0. The remaining ones are less than 0.1. The smallest ratio is for the dipole-allowed excitation to the level No. 59 which has the largest magnitude of direct-excitation rate coefficients of the 106 transitions.

(4) At the temperature of 2500 eV, the ratios are still larger than 1.0 for 15 transitions. The largest one is 3.8 for the level No. 4. The ratios are between 0.1 and 1.0 for 73 transitions.

TABLE IV. Direct electron-impact excitation-rate coefficients (DE) and resonant contributions (RE) in $cm^3\ s^{-1}$ from the ground state of Ni-like Ta ($a[-b]=a\times10^{-b}$).

Excited level		Temperature (eV)					Excited level		Temperature (eV)				
		400	800	1200	1500	2500			400	800	1200	1500	2500
2	DE	5.13[−14]	2.12[−13]	2.94[−13]	3.16[−13]	3.04[−13]	55	DE	2.24[−14]	1.89[−13]	3.35[−13]	4.02[−13]	4.77[−13]
	RE	4.50[−13]	1.30[−12]	1.45[−12]	1.39[−12]	1.03[−12]		RE	3.26[−14]	1.99[−13]	2.83[−13]	2.98[−13]	2.57[−13]
3	DE	1.57[−13]	7.54[−13]	1.19[−12]	1.39[−12]	1.71[−12]	56	DE	2.69[−14]	2.51[−13]	4.83[−13]	6.10[−13]	8.26[−13]
	RE	5.77[−13]	1.73[−12]	1.96[−12]	1.89[−12]	1.42[−12]		RE	2.77[−14]	1.71[−13]	2.45[−13]	2.58[−13]	2.23[−13]
4	DE	1.99[−14]	8.84[−14]	1.25[−13]	1.36[−13]	1.33[−13]	57	DE	4.38[−14]	4.02[−13]	7.62[−13]	9.52[−13]	1.25[−12]
	RE	1.81[−13]	5.79[−13]	6.71[−13]	6.53[−13]	4.99[−13]		RE	3.87[−14]	2.38[−13]	3.39[−13]	3.57[−13]	3.09[−13]
5	DE	9.38[−14]	4.80[−13]	7.68[−13]	9.04[−13]	1.11[−12]	58	DE	1.95[−14]	1.58[−13]	2.69[−13]	3.12[−13]	3.32[−13]
	RE	4.62[−13]	1.46[−12]	1.68[−12]	1.63[−12]	1.24[−12]		RE	3.36[−14]	2.08[−13]	2.96[−13]	3.11[−13]	2.69[−13]
6	DE	4.15[−14]	1.95[−13]	2.83[−13]	3.10[−13]	3.07[−13]	59	DE	2.35[−12]	2.48[−11]	5.18[−11]	6.87[−11]	1.05[−10]
	RE	2.42[−13]	7.93[−13]	9.23[−13]	8.97[−13]	6.84[−13]		RE	7.41[−14]	4.58[−13]	6.51[−13]	6.86[−13]	5.92[−13]
7	DE	7.10[−14]	3.59[−13]	5.58[−13]	6.44[−13]	7.45[−13]	60	DE	1.09[−14]	9.91[−14]	1.79[−13]	2.14[−13]	2.43[−13]
	RE	2.44[−13]	8.07[−13]	9.39[−13]	9.14[−13]	6.97[−13]		RE	2.02[−14]	1.27[−13]	1.82[−13]	1.93[−13]	1.68[−13]
8	DE	2.74[−14]	1.37[−13]	2.02[−13]	2.22[−13]	2.21[−13]	61	DE	6.44[−15]	5.82[−14]	1.05[−13]	1.25[−13]	1.42[−13]
	RE	1.67[−13]	5.92[−13]	7.05[−13]	6.93[−13]	5.36[−13]		RE	1.57[−14]	9.97[−14]	1.44[−13]	1.53[−13]	1.34[−13]
9	DE	1.26[−13]	8.10[−13]	1.47[−12]	1.86[−12]	2.68[−12]	62	DE	2.09[−14]	2.27[−13]	4.73[−13]	6.24[−13]	9.31[−13]
	RE	8.23[−13]	2.95[−12]	3.52[−12]	3.45[−12]	2.66[−12]		RE	2.00[−14]	1.25[−13]	1.79[−13]	1.90[−13]	1.65[−13]
10	DE	4.37[−14]	2.28[−13]	3.41[−13]	3.78[−13]	3.81[−13]	63	DE	4.18[−13]	4.47[−12]	9.09[−12]	1.17[−11]	1.65[−11]
	RE	1.59[−13]	5.64[−13]	6.72[−13]	6.59[−13]	5.10[−13]		RE	3.90[−14]	2.62[−13]	3.85[−13]	4.11[−13]	3.63[−13]
11	DE	2.64[−14]	1.39[−13]	2.09[−13]	2.32[−13]	2.34[−13]	64	DE	1.47[−15]	1.51[−14]	2.83[−14]	3.45[−14]	4.00[−14]
	RE	1.54[−13]	5.49[−13]	6.55[−13]	6.44[−13]	5.00[−13]		RE	3.32[−15]	2.27[−14]	3.35[−14]	3.58[−14]	3.18[−14]
12	DE	1.72[−13]	1.18[−12]	2.20[−12]	2.82[−12]	4.22[−12]	65	DE	8.92[−15]	1.09[−13]	2.41[−13]	3.28[−13]	5.26[−13]
	RE	7.20[−13]	2.51[−12]	2.94[−12]	2.87[−12]	2.19[−12]		RE	3.25[−14]	2.14[−13]	3.11[−13]	3.29[−13]	2.88[−13]
13	DE	3.19[−14]	1.83[−13]	2.97[−13]	3.48[−13]	4.15[−13]	66	DE	1.84[−15]	2.00[−14]	3.84[−14]	4.71[−14]	5.54[−14]
	RE	1.28[−13]	4.61[−13]	5.53[−13]	5.45[−13]	4.24[−13]		RE	3.11[−15]	2.19[−14]	3.27[−14]	3.50[−14]	3.12[−14]
14	DE	8.12[−15]	4.64[−14]	7.19[−14]	8.11[−14]	8.39[−14]	67	DE	9.12[−15]	1.16[−13]	2.56[−13]	3.46[−13]	5.42[−13]
	RE	2.63[−14]	1.03[−13]	1.26[−13]	1.25[−13]	9.87[−14]		RE	9.76[−15]	6.90[−14]	1.03[−13]	1.10[−13]	9.81[−14]
15	DE	2.75[−14]	1.81[−13]	3.19[−13]	3.94[−13]	5.35[−13]	68	DE	1.82[−14]	2.24[−13]	4.77[−13]	6.27[−13]	9.12[−13]
	RE	1.80[−13]	6.76[−13]	8.15[−13]	8.02[−13]	6.23[−13]		RE	1.09[−14]	7.96[−14]	1.21[−13]	1.30[−13]	1.17[−13]
16	DE	3.95[−14]	2.43[−13]	4.04[−13]	4.79[−13]	5.78[−13]	69	DE	3.59[−15]	3.90[−14]	7.42[−14]	9.07[−14]	1.06[−13]
	RE	1.35[−13]	5.24[−13]	6.44[−13]	6.39[−13]	5.04[−13]		RE	1.07[−14]	7.68[−14]	1.15[−13]	1.24[−13]	1.11[−13]
17	DE	1.37[−14]	7.77[−14]	1.19[−13]	1.33[−13]	1.35[−13]	70	DE	8.88[−15]	9.84[−14]	1.89[−13]	2.32[−13]	2.72[−13]
	RE	1.01[−13]	3.97[−13]	4.90[−13]	4.88[−13]	3.86[−13]		RE	1.18[−14]	8.70[−14]	1.32[−13]	1.43[−13]	1.29[−13]
18	DE	4.90[−14]	3.04[−13]	4.80[−13]	5.45[−13]	5.69[−13]	71	DE	4.94[−15]	5.54[−14]	1.07[−13]	1.32[−13]	1.55[−13]
	RE	7.80[−14]	3.16[−13]	3.92[−13]	3.90[−13]	3.09[−13]		RE	1.40[−14]	1.04[−13]	1.57[−13]	1.69[−13]	1.52[−13]
19	DE	5.02[−14]	3.22[−13]	5.26[−13]	6.10[−13]	6.85[−13]	72	DE	9.04[−14]	1.32[−12]	3.17[−12]	4.50[−12]	7.87[−12]
	RE	6.72[−14]	2.84[−13]	3.58[−13]	3.60[−13]	2.88[−13]		RE	4.06[−14]	2.83[−13]	4.17[−13]	4.46[−13]	3.94[−13]
20	DE	5.18[−14]	3.40[−13]	5.68[−13]	6.69[−13]	7.84[−13]	73	DE	9.54[−15]	1.21[−13]	2.61[−13]	3.46[−13]	5.08[−13]
	RE	8.44[−14]	3.47[−13]	4.33[−13]	4.32[−13]	3.44[−13]		RE	9.78[−15]	7.40[−14]	1.13[−13]	1.23[−13]	1.11[−13]
21	DE	3.22[−14]	1.97[−13]	3.08[−13]	3.47[−13]	3.54[−13]	74	DE	3.69[−15]	4.22[−14]	8.19[−14]	1.01[−13]	1.19[−13]
	RE	6.78[−14]	2.87[−13]	3.62[−13]	3.63[−13]	2.91[−13]		RE	6.27[−15]	4.99[−14]	7.78[−14]	8.50[−14]	7.82[−14]
22	DE	3.40[−14]	2.15[−13]	3.42[−13]	3.88[−13]	4.04[−13]	75	DE	1.32[−13]	1.77[−12]	3.90[−12]	5.19[−12]	7.68[−12]
	RE	7.86[−14]	3.30[−13]	4.14[−13]	4.15[−13]	3.31[−13]		RE	1.26[−14]	1.05[−13]	1.66[−13]	1.83[−13]	1.69[−13]
23	DE	6.34[−14]	3.98[−13]	6.30[−13]	7.13[−13]	7.36[−13]	76	DE	4.04[−15]	5.23[−14]	1.06[−13]	1.33[−13]	1.62[−13]
	RE	8.34[−14]	3.56[−13]	4.51[−13]	4.53[−13]	3.64[−13]		RE	4.97[−15]	4.35[−14]	6.97[−14]	7.70[−14]	7.18[−14]
24	DE	4.15[−14]	2.62[−13]	4.15[−13]	4.69[−13]	4.85[−13]	77	DE	1.10[−14]	1.67[−13]	3.88[−13]	5.33[−13]	8.47[−13]
	RE	8.40[−14]	3.63[−13]	4.60[−13]	4.63[−13]	3.73[−13]		RE	5.83[−15]	5.07[−14]	8.13[−14]	8.98[−14]	8.39[−14]

TABLE IV. (*Continued.*)

Excited level		Temperature (eV) 400	800	1200	1500	2500	Excited level		Temperature (eV) 400	800	1200	1500	2500
25	DE	9.60[−14]	7.16[−13]	1.30[−12]	1.62[−12]	2.17[−12]	78	DE	7.68[−15]	1.02[−13]	2.06[−13]	2.59[−13]	3.14[−13]
	RE	9.52[−14]	4.02[−13]	5.07[−13]	5.08[−13]	4.07[−13]		RE	2.03[−15]	2.02[−14]	3.37[−14]	3.78[−14]	3.61[−14]
26	DE	3.15[−14]	2.03[−13]	3.27[−13]	3.75[−13]	4.07[−13]	79	DE	1.02[−14]	1.38[−13]	2.86[−13]	3.62[−13]	4.56[−13]
	RE	6.20[−14]	2.73[−13]	3.50[−13]	3.54[−13]	2.86[−13]		RE	4.11[−15]	4.03[−14]	6.70[−14]	7.50[−14]	7.14[−14]
27	DE	1.77[−13]	1.32[−12]	2.37[−12]	2.90[−12]	3.73[−12]	80	DE	1.06[−14]	1.60[−13]	3.62[−13]	4.89[−13]	7.34[−13]
	RE	8.73[−14]	4.13[−13]	5.40[−13]	5.50[−13]	4.51[−13]		RE	5.96[−15]	5.68[−14]	9.34[−14]	1.04[−13]	9.86[−14]
28	DE	2.51[−14]	1.68[−13]	2.71[−13]	3.10[−13]	3.27[−13]	81	DE	1.12[−14]	1.50[−13]	3.07[−13]	3.86[−13]	4.71[−13]
	RE	5.99[−14]	2.70[−13]	3.47[−13]	3.51[−13]	2.85[−13]		RE	6.54[−15]	6.24[−14]	1.03[−13]	1.14[−13]	1.08[−13]
29	DE	3.28[−14]	2.18[−13]	3.51[−13]	4.00[−13]	4.19[−13]	82	DE	5.53[−15]	7.33[−14]	1.48[−13]	1.85[−13]	2.23[−13]
	RE	5.44[−14]	2.49[−13]	3.24[−13]	3.29[−13]	2.68[−13]		RE	4.82[−15]	4.65[−14]	7.68[−14]	8.58[−14]	8.14[−14]
30	DE	5.42[−14]	4.25[−13]	7.87[−13]	9.83[−13]	1.33[−12]	83	DE	6.84[−15]	9.15[−14]	1.86[−13]	2.33[−13]	2.83[−13]
	RE	6.12[−14]	2.77[−13]	3.57[−13]	3.62[−13]	2.94[−13]		RE	6.54[−15]	6.29[−14]	1.04[−13]	1.16[−13]	1.10[−13]
31	DE	2.99[−14]	2.05[−13]	3.35[−13]	3.85[−13]	4.09[−13]	84	DE	5.55[−15]	8.53[−14]	1.96[−13]	2.67[−13]	4.11[−13]
	RE	5.34[−14]	2.43[−13]	3.12[−13]	3.16[−13]	2.56[−13]		RE	6.50[−15]	6.28[−14]	1.04[−13]	1.16[−13]	1.10[−13]
32	DE	3.83[−14]	2.71[−13]	4.55[−13]	5.33[−13]	6.06[−13]	85	DE	1.41[−13]	2.33[−12]	5.63[−12]	7.87[−12]	1.30[−11]
	RE	5.76[−14]	2.73[−13]	3.59[−13]	3.66[−13]	3.00[−13]		RE	9.55[−15]	9.50[−14]	1.59[−13]	1.78[−13]	1.70[−13]
33	DE	4.15[−14]	3.07[−13]	5.38[−13]	6.48[−13]	7.96[−13]	86	DE	1.09[−15]	1.51[−14]	3.14[−14]	3.97[−14]	4.94[−14]
	RE	7.31[−14]	3.40[−13]	4.42[−13]	4.49[−13]	3.66[−13]		RE	3.58[−15]	3.37[−14]	5.56[−14]	6.21[−14]	5.91[−14]
34	DE	2.45[−14]	1.66[−13]	2.68[−13]	3.06[−13]	3.19[−13]	87	DE	6.47[−14]	1.04[−12]	2.42[−12]	3.31[−12]	5.10[−12]
	RE	5.95[−14]	2.85[−13]	3.74[−13]	3.82[−13]	3.15[−13]		RE	4.67[−15]	4.75[−14]	8.05[−14]	9.11[−14]	8.82[−14]
35	DE	1.16[−14]	8.27[−14]	1.37[−13]	1.58[−13]	1.70[−13]	88	DE	1.08[−14]	2.21[−13]	6.04[−13]	9.09[−13]	1.79[−12]
	RE	5.18[−14]	2.52[−13]	3.33[−13]	3.40[−13]	2.81[−13]		RE	4.77[−15]	4.70[−14]	7.82[−14]	8.75[−14]	8.34[−14]
36	DE	1.16[−12]	9.48[−12]	1.76[−11]	2.18[−11]	2.87[−11]	89	DE	3.94[−16]	6.11[−15]	1.32[−14]	1.69[−14]	2.16[−14]
	RE	8.82[−14]	4.64[−13]	6.29[−13]	6.50[−13]	5.45[−13]		RE	5.14[−16]	5.47[−15]	9.36[−15]	1.06[−14]	1.03[−14]
37	DE	9.35[−14]	8.80[−13]	1.84[−12]	2.46[−12]	3.96[−12]	90	DE	1.12[−15]	1.73[−14]	3.70[−14]	4.73[−14]	5.98[−14]
	RE	2.79[−13]	1.35[−12]	1.76[−12]	1.80[−12]	1.47[−12]		RE	1.99[−15]	2.03[−14]	3.41[−14]	3.84[−14]	3.70[−14]
38	DE	1.97[−14]	1.49[−13]	2.51[−13]	2.92[−13]	3.15[−13]	91	DE	3.39[−15]	6.89[−14]	1.85[−13]	2.75[−13]	5.26[−13]
	RE	8.14[−15]	4.47[−14]	6.14[−14]	6.36[−14]	5.37[−14]		RE	5.58[−15]	5.53[−14]	9.20[−14]	1.03[−13]	9.84[−14]
39	DE	4.99[−14]	3.84[−13]	6.56[−13]	7.69[−13]	8.55[−13]	92	DE	2.52[−15]	4.06[−14]	8.89[−14]	1.15[−13]	1.49[−13]
	RE	1.76[−14]	1.00[−13]	1.39[−13]	1.45[−13]	1.23[−13]		RE	4.88[−15]	4.89[−14]	8.17[−14]	9.16[−14]	8.76[−14]
40	DE	3.13[−14]	2.42[−13]	4.19[−13]	4.96[−13]	5.78[−13]	93	DE	5.43[−15]	9.67[−14]	2.31[−13]	3.18[−13]	4.94[−13]
	RE	2.70[−14]	1.52[−13]	2.11[−13]	2.19[−13]	1.86[−13]		RE	2.81[−15]	2.93[−14]	4.99[−14]	5.65[−14]	5.48[−14]
41	DE	4.69[−14]	3.54[−13]	5.94[−13]	6.87[−13]	7.33[−13]	94	DE	1.09[−15]	1.89[−14]	4.23[−14]	5.51[−14]	7.18[−14]
	RE	2.51[−14]	1.44[−13]	2.01[−13]	2.09[−13]	1.78[−13]		RE	1.73[−15]	2.05[−14]	3.64[−14]	4.20[−14]	4.19[−14]
42	DE	5.14[−14]	3.88[−13]	6.48[−13]	7.48[−13]	7.94[−13]	95	DE	2.75[−15]	6.32[−14]	1.80[−13]	2.77[−13]	5.71[−13]
	RE	3.49[−14]	1.98[−13]	2.75[−13]	2.86[−13]	2.43[−13]		RE	2.33[−15]	2.64[−14]	4.63[−14]	5.29[−14]	5.22[−14]
43	DE	3.79[−14]	2.93[−13]	5.01[−13]	5.88[−13]	6.59[−13]	96	DE	2.43[−15]	4.64[−14]	1.07[−13]	1.41[−13]	1.87[−13]
	RE	2.70[−14]	1.53[−13]	2.12[−13]	2.21[−13]	1.87[−13]		RE	8.58[−16]	1.14[−14]	2.10[−14]	2.45[−14]	2.49[−14]
44	DE	2.47[−14]	1.84[−13]	3.04[−13]	3.49[−13]	3.65[−13]	97	DE	4.39[−15]	8.41[−14]	1.93[−13]	2.54[−13]	3.35[−13]
	RE	2.62[−14]	1.50[−13]	2.08[−13]	2.17[−13]	1.84[−13]		RE	1.50[−15]	2.07[−14]	3.85[−14]	4.51[−14]	4.62[−14]
45	DE	3.65[−14]	2.76[−13]	4.61[−13]	5.33[−13]	5.66[−13]	98	DE	3.99[−14]	9.40[−13]	2.56[−12]	3.76[−12]	6.72[−12]
	RE	8.86[−14]	4.73[−13]	6.42[−13]	6.63[−13]	5.54[−13]		RE	1.08[−15]	1.54[−14]	2.90[−14]	3.41[−14]	3.53[−14]
46	DE	3.70[−14]	2.80[−13]	4.67[−13]	5.39[−13]	5.70[−13]	99	DE	3.52[−15]	7.60[−14]	1.94[−13]	2.73[−13]	4.43[−13]
	RE	3.20[−14]	1.82[−13]	2.53[−13]	2.63[−13]	2.24[−13]		RE	1.32[−15]	1.74[−14]	3.18[−14]	3.70[−14]	3.75[−14]
47	DE	1.91[−14]	1.44[−13]	2.42[−13]	2.81[−13]	3.09[−13]	100	DE	5.33[−16]	1.11[−14]	2.63[−14]	3.51[−14]	4.77[−14]
	RE	3.40[−14]	1.92[−13]	2.66[−13]	2.77[−13]	2.35[−13]		RE	6.87[−16]	9.21[−15]	1.70[−14]	1.98[−14]	2.02[−14]
48	DE	7.07[−14]	6.40[−13]	1.24[−12]	1.58[−12]	2.19[−12]	101	DE	1.67[−15]	4.02[−14]	1.08[−13]	1.57[−13]	2.70[−13]

TABLE IV. (*Continued.*)

Excited level		Temperature (eV) 400	800	1200	1500	2500	Excited level		Temperature (eV) 400	800	1200	1500	2500
	RE	5.21[−14]	2.91[−13]	4.00[−13]	4.16[−13]	3.52[−13]		RE	1.54[−15]	2.07[−14]	3.83[−14]	4.47[−14]	4.56[−14]
49	DE	9.32[−13]	9.03[−12]	1.83[−11]	2.40[−11]	3.59[−11]	102	DE	1.09[−15]	2.34[−14]	5.63[−14]	7.56[−14]	1.04[−13]
	RE	9.38[−14]	5.32[−13]	7.36[−13]	7.65[−13]	6.47[−13]		RE	1.51[−15]	2.08[−14]	3.88[−14]	4.54[−14]	4.66[−14]
50	DE	6.99[−15]	5.56[−14]	9.57[−14]	1.12[−13]	1.24[−13]	103	DE	4.61[−15]	1.20[−13]	3.39[−13]	5.05[−13]	9.26[−13]
	RE	2.42[−14]	1.35[−13]	1.87[−13]	1.95[−13]	1.65[−13]		RE	2.26[−15]	3.06[−14]	5.64[−14]	6.59[−14]	6.72[−14]
51	DE	4.31[−14]	4.07[−13]	8.07[−13]	1.04[−12]	1.48[−12]	104	DE	1.23[−15]	3.18[−14]	8.10[−14]	1.11[−13]	1.58[−13]
	RE	4.75[−14]	2.63[−13]	3.63[−13]	3.77[−13]	3.19[−13]		RE	2.22[−16]	4.13[−15]	8.49[−15]	1.04[−14]	1.13[−14]
52	DE	2.74[−14]	2.22[−13]	3.80[−13]	4.43[−13]	4.78[−13]	105	DE	2.62[−15]	7.37[−14]	2.02[−13]	2.92[−13]	4.82[−13]
	RE	2.25[−14]	1.38[−13]	1.96[−13]	2.06[−13]	1.78[−13]		RE	3.71[−16]	6.94[−15]	1.43[−14]	1.75[−14]	1.91[−14]
53	DE	4.01[−14]	3.29[−13]	5.67[−13]	6.63[−13]	7.22[−13]	106	DE	2.15[−15]	5.60[−14]	1.43[−13]	1.97[−13]	2.81[−13]
	RE	3.72[−14]	2.36[−13]	3.38[−13]	3.57[−13]	3.11[−13]		RE	5.39[−16]	9.98[−15]	2.05[−14]	2.49[−14]	2.72[−14]
54	DE	3.10[−14]	2.55[−13]	4.38[−13]	5.12[−13]	5.55[−13]	107	DE	9.11[−15]	2.84[−13]	8.39[−13]	1.27[−12]	2.33[−12]
	RE	3.02[−14]	1.93[−13]	2.78[−13]	2.94[−13]	2.56[−13]		RE	4.40[−16]	8.27[−15]	1.71[−14]	2.08[−14]	2.28[−14]

G. Comparison with other works

The dielectronic recombination rate coefficients are calculated using the same set of basic atomic data as those involved in the calculation of RE rates, such as energy levels, Auger, and radiative rates. The comparison between the DR rate coefficients using the present basic atomic data with the existing DR rates can give an overall check. The present total DR rates of Ni-like Ta^{45+} ion through the resonances associated with $3l \rightarrow 4l'$ core excitations are found to agree well with the results calculated using the HULLAC code package [22] to within 10% at temperatures $100\ \text{eV} \leqslant kT \leqslant 10\,000$ eV. It should be pointed out that the contributions from the resonances associated with $3l \rightarrow 5l'$ core excitations enlarge the DR rate coefficients by a factor of 10%–20% for temperatures above 1 keV.

Chen and Osterheld [14] presented the direct and resonant excitation rate coefficients to the 54 levels of the $3d^9 4l$ configurations of Ta^{45+}. We compare the present excitation rate coefficients to energy levels Nos. 9 and 12 with the rates from Ref. [14] in Figs. 4(a) and 4(b). As can be seen from Fig. 4, the present DE rates agree with Chen's within 10% for most transitions. The present RE rate coefficients at $kT = 1200$ eV to levels No. 9 and No. 12 are larger than Chen's [14] by 79% and 53%. The corresponding total excitation rates are about 46% and 31% higher than Chen's. Large discrepancies up to 150% between the present and Chen's RE rates are also found for other levels of the $3d^9 4s$ and $3d^9 4p$ configurations. For all levels belonging to the $3d^9 4s$ and $3d^9 4p$ configurations, the present RE rates are higher than Chen's. This is manly because the RE contributions through the $3d^9 4l' n'' l''$ complex series are included in the present calculation, and this complex series contributes significantly only to the low-lying levels of the $3d^9 4l$ configurations. For example, $3d^9 4l' n'' l''$ complexes contribute about 40% to the total RE rate coefficients for both levels No. 9 and No. 12. For most of the $3d^9 4d$ and $3d^9 4f$ levels, the present RE rates are less than Chen's by up to 50%. This is mainly due to the

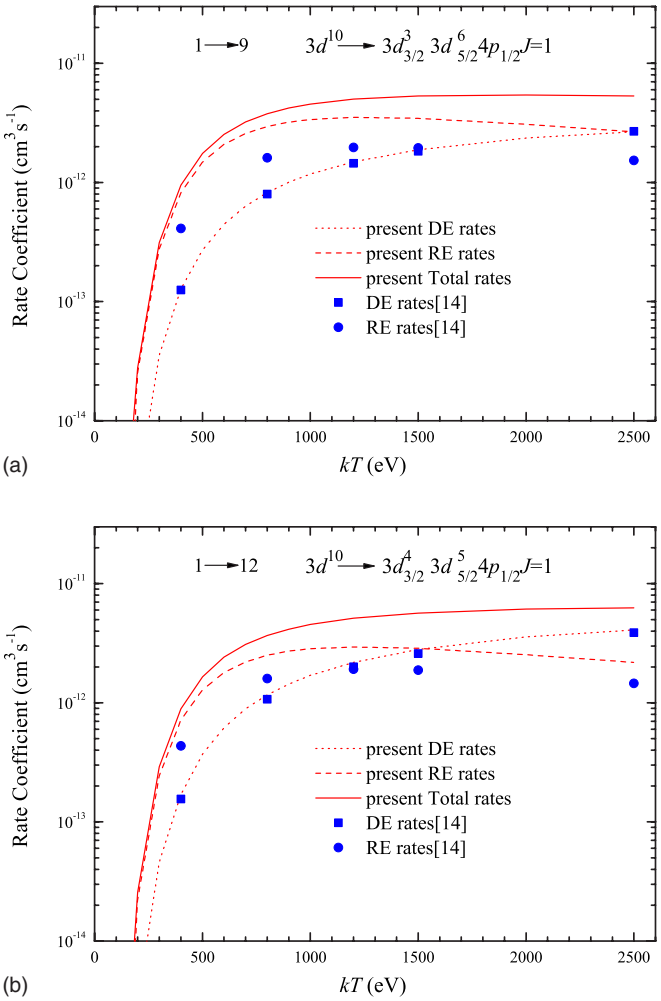

FIG. 4. (Color online) Excitation rate coefficients from the ground state of Ta^{45+} to energy levels No. 9 (a) and No. 12 (b) as functions of the electron temperature. For comparison, the DE and RE rate coefficients from Ref. [14] are also plotted.

present inclusion of DAC effects as discussed in Sec. III E. It is interesting that the deviations are found to be only few percents for eleven transitions, such as No. $1 \rightarrow 28, 29, 32$, etc. This good agreement may be somewhat fortuitous.

IV. CONCLUSION

In conclusion, a detailed and large-scale calculation on the resonant excitation rate coefficients from the ground state to the 106 fine-structure levels belonging to the $3l^{17}4l'$ ($l=0,1,2$; $l'=0,1,2,3$) configurations of Ni-like tantalum have been performed using the recently developed atomic code FAC. The contributions through all possible Cu-like doubly excited states $3l^{17}4l'n''l''$ and $3l^{17}5l'n''l''$ are included. The contributions from high n'' Rydberg states are found to follow approximately the n''^{-3} scaling law with $n'' \geqslant 14$. The $3d^9 4l'n''l''$ complex series contributes significantly to the resonant excitation rate coefficients of low-lying levels in the $3d^9 4l'$ configurations. The resonances associated with $3l \rightarrow 5l'$ core excitations dominate the RE rates for high-lying singly excited states. The radiative damping effects are significant for the transitions into levels of the $3d^9 4l'$ configurations, and negligible for transitions into the $3p^5 4l'$ and $3s4l'$ states. The inclusion of DAC transitions reduces significantly the RE rates of most transitions from the ground state to the $3l^{17}4l'$ states. The contributions from resonant excitation are found to be as important as the direct excitation processes for many transitions. In some cases, the resonant excitation can enhance the excitation rate coefficients by an order of magnitude. Large discrepancies between the present RE rate coefficients and the existing values are found. We believe that the present results should be more reliable and accurate.

ACKNOWLEDGMENTS

This work is supported by the National Natural Science Foundation of China under Grants No. 10574029 and No. 10434050, the Chinese Association of Atomic and Molecular Data, and National High-Tech ICF Committee in China. One of the authors (M.F.G.) gratefully acknowledges the support from Fudan University.

[1] B. J. MacGowan, S. Maxon, L. B. Da Silva, D. J. Fields, C. J. Keane, D. L. Matthews, A. L. Osterheld, J. H. Scofield, G. Shimkaveg, and G. G. Stone, Phys. Rev. Lett. **65**, 420 (1990).
[2] M. E. Foord, S. H. Glenzer, R. S. Thoe, K. L. Wong, K. B. Fournier, B. G. Wilson, and P. T. Springer, Phys. Rev. Lett. **85**, 992 (2000).
[3] M. J. May *et al.*, Nucl. Instrum. Methods Phys. Res. B **235**, 231 (2005).
[4] P. L. Hagelstein, Phys. Rev. A **34**, 874 (1986).
[5] H. L. Zhang, D. H. Sampson, and A. K. Mohanty, Phys. Rev. A **40**, 616 (1989).
[6] H. L. Zhang, D. H. Sampson, and C. J. Fontes, At. Data Nucl. Data Tables **48**, 91 (1991).
[7] J. Y. Zhong, C. Wang, J. Zhang, X. Lu, G. Zhao, J. L. Zeng, M. F. Gu, and S. J. Wang, Phys. Rev. A **70**, 053803 (2004).
[8] J. Zhong, J. Zhang, J. L. Zeng, G. Zhao, and M. F. Gu, At. Data Nucl. Data Tables **89**, 101 (2005).
[9] K. M. Aggarwal, P. H. Norrington, K. L. Bell, F. P. Keenan, G. J. Pert, and S. J. Rose, J. Phys. B **32**, 5067 (1999).
[10] K. M. Aggarwal, F. P. Keenan, P. H. Norrington, G. J. Pert, and S. J. Rose, J. Phys. B **35**, L127 (2002).
[11] K. M. Aggarwal, F. P. Keenan, R. Kisielius, P. H. Norrington, R. E. King, G. J. Pert, and S. J. Rose, Phys. Scr. **71**, 356 (2005).
[12] N. R. Badnell, K. A. Berrington, H. P. Summers, M. G. O'Mullane, A. D. Whiteford, and C. P. Ballance, J. Phys. B **37**, 4589 (2004).
[13] C. P. Ballance and D. C. Griffin, J. Phys. B **39**, 3617 (2006).
[14] M. H. Chen and A. L. Osterheld, Phys. Rev. A **52**, 3790 (1995).
[15] K. B. Fournier, W. H. Goldstein, M. May, M. Finkenthal, and J. L. Terry, Phys. Rev. A **53**, 3110 (1996).
[16] J. Oreg, W. Goldstein, P. Mandelbaum, D. Mitnik, E. Meroz, J. L. Schwob, and A. Bar Shalom, Phys. Rev. A **44**, 1741 (1991).
[17] M. F. Gu, Astrophys. J. **582**, 1241 (2003).
[18] M. F. Gu, Astrophys. J. **589**, 1085 (2003).
[19] M. F. Gu, Astrophys. J. **590**, 1131 (2003).
[20] A. Bar-Shalom, M. Klapisch, and J. Oreg, Phys. Rev. A **38**, 1773 (1988).
[21] Y. Hahn, Adv. At. Mol. Phys. **21**, 123 (1985).
[22] E. Behar, P. Mandelbaum, J. L. Schwob, A. Bar-Shalom, J. Oreg, and W. H. Goldstein, Phys. Rev. A **54**, 3070 (1996).
[23] E. Behar, P. Mandelbaum, J. L. Schwob, A. Bar-Shalom, J. Oreg, and W. H. Goldstein, Phys. Rev. A **52**, 3770 (1995).
[24] D. Coster and R. de L. Kronig, Physica (Amsterdam) **2**, 13 (1935).
[25] E. J. Mcguire, Phys. Rev. A **5**, 1043 (1972).